

Galaxy And Mass Assembly (GAMA): AUTOZ spectral redshift measurements, confidence and errors.

I. K. Baldry,¹ M. Alpaslan,^{2,3} A. E. Bauer,⁴ J. Bland-Hawthorn,⁵ S. Brough,⁴
 M. E. Cluver,⁶ S. M. Croom,⁵ L. J. M. Davies,² S. P. Driver,^{2,3} M. L. P. Gunawardhana,⁷
 B. W. Holwerda,⁸ A. M. Hopkins,⁴ L. S. Kelvin,⁹ J. Liske,¹⁰ Á. R. López-Sánchez,^{4,11}
 J. Loveday,¹² P. Norberg,⁷ J. Peacock,¹³ A. S. G. Robotham,² E. N. Taylor¹⁴

¹*Astrophysics Research Institute, Liverpool John Moores University, IC2, Liverpool Science Park, 146 Brownlow Hill, Liverpool L3 5RF*

²*International Centre for Radio Astronomy Research, University of Western Australia, 35 Stirling Highway, Crawley, WA 6009, Australia*

³*School of Physics and Astronomy, University of St Andrews, North Haugh, St Andrews KY16 9SS*

⁴*Australian Astronomical Observatory, PO Box 915, North Ryde, NSW 1670, Australia*

⁵*Sydney Institute for Astronomy, School of Physics A28, University of Sydney, NSW 2006, Australia*

⁶*Department of Astronomy, University of Cape Town, Private Bag X3, Rondebosch, 7701, South Africa*

⁷*ICC, Department of Physics, Durham University, South Road, Durham DH1 3LE*

⁸*University of Leiden, Sterrenwacht Leiden, Niels Bohrweg 2, NL-2333 CA Leiden, Netherlands*

⁹*Institut für Astro- und Teilchenphysik, Universität Innsbruck, Technikerstraße 25, 6020 Innsbruck, Austria*

¹⁰*European Southern Observatory, Karl-Schwarzschild-Str. 2, 85748 Garching, Germany*

¹¹*Department of Physics and Astronomy, Macquarie University, NSW 2109, Australia*

¹²*Astronomy Centre, University of Sussex, Falmer, Brighton BN1 9QH*

¹³*Institute for Astronomy, University of Edinburgh, Royal Observatory, Blackford Hill, Edinburgh EH9 3HJ*

¹⁴*School of Physics, University of Melbourne, Parkville, VIC 3010, Australia*

Paper submitted to MNRAS on 2014 February 26th; revised following referee comments, 2014 April 8th.

ABSTRACT

The Galaxy And Mass Assembly (GAMA) survey has obtained spectra of over 230 000 targets using the Anglo-Australian Telescope. To homogenise the redshift measurements and improve the reliability, a fully automatic redshift code was developed (AUTOZ). The measurements were made using a cross-correlation method for both absorption-line and emission-line spectra. Large deviations in the high-pass filtered spectra are partially clipped in order to be robust against uncorrected artefacts and to reduce the weight given to single-line matches. A single figure of merit (FOM) was developed that puts all template matches onto a similar confidence scale. The redshift confidence as a function of the FOM was fitted with a tanh function using a maximum likelihood method applied to repeat observations of targets. The method could be adapted to provide robust automatic redshifts for other large galaxy redshift surveys. For the GAMA survey, there was a substantial improvement in the reliability of assigned redshifts and in the lowering of redshift uncertainties with a median velocity uncertainty of 33 km/s.

Key words: methods: data analysis — techniques: spectroscopic — surveys — galaxies: redshifts

1 INTRODUCTION

Spectroscopic redshift measurements of large galaxy samples form the backbone of many extragalactic and cosmological analyses. They are key for testing cosmological models, e.g. using redshift space distortions (Kaiser 1987), and for providing distances for galaxy population studies when the cosmology is assumed. Redshifts from spectroscopy (spec- z) generally have significantly fewer outliers, compared to the true redshift, than from photometric estimates (photo- z ; Dahlen et al. 2013). In addition, spec- z mea-

surements are essential for accurate low-redshift luminosity estimates ($0.002 \lesssim z \lesssim 0.2$), where the photo- z fractional error is too large, and for dynamical measurements within groups of galaxies (Beers, Flynn, & Gebhardt 1990, Robotham et al. 2011).

Redshift surveys of large numbers of galaxies have been undertaken in recent years using multi-object spectrographs such as the Two Degree Field (2dF, Lewis et al. 2002), Sloan Digital Sky Survey (SDSS, Smee et al. 2013), Visible Multi-Object Spectrograph (VIMOS, Le Fèvre et al. 2003), and Deep Imaging Multi-Object Spectrograph (DEIMOS, Faber et al. 2003). For uniformity

of a survey product over a large sample, redshift measurement codes have been developed that are either fully automatic (SubbaRao et al. 2002; Garilli et al. 2010; Bolton et al. 2012) or partially automatic with some user interaction (Colless et al. 2001; Newman et al. 2013).

The main techniques for spectroscopic redshift measurements are: the identification and fitting of spectral features (Mink & Wyatt 1995); cross-correlation of observed spectra with template spectra (Tonry & Davis 1979; Kurtz et al. 1992); and χ^2 fitting using linear combinations of eigenspectra (Glazebrook, Offer, & Deeley 1998). A widely used code is RVSAO that allows for cross-correlation with absorption-line and emission-line templates separately (Kurtz & Mink 1998). The 2dF Galaxy Redshift Survey (2dFGRS) and SDSS have used a dual method with fitting of emission line features and cross-correlation with templates after clipping the identified emission lines from the observed spectra (Colless et al. 2001; Stoughton et al. 2002). The large VIMOS surveys have used the EZ software (Garilli et al. 2010), which provides a number of options including emission-line finding, cross-correlation and χ^2 fitting. From SDSS Data Release 8 (DR8) onwards (Aihara et al. 2011), including the Baryon Oscillation Spectroscopic Survey (BOSS) targets, the measurements have used χ^2 fitting at trial redshifts with sets of eigenspectra for galaxies and quasars (Bolton et al. 2012).

The Galaxy And Mass Assembly (GAMA) survey is based around a redshift survey that was designed, in large part, for finding and characterising groups of galaxies (Driver et al. 2009; Robotham et al. 2011). The survey has obtained over 200 000 redshifts using spectra from the AAOmega spectrograph of the Anglo-Australian Telescope (AAT) fed by the 2dF fibre positioner. AAOmega is a bench-mounted spectrograph with light coming from a 392-fibre slit, split into two beams, each dispersed with a volume-phase holographic grating and focused onto CCDs using a Schmidt camera. See Sharp et al. (2006) for details.

Up until 2013, all the AAOmega redshifts had been obtained using RUNZ (Saunders, Cannon, & Sutherland 2004), which is an update to the code used by the 2dFGRS (Colless et al. 2001). The user assigns a redshift quality for each spectrum from 1–4, which can later be changed or normalised during a quality control process (Driver et al. 2011). By comparing the redshifts assigned to repeated AAOmega observations of the same target, the typical redshift uncertainty was estimated to be ~ 100 km/s. In addition, the blunder rate was ~ 5 per cent even when the redshifts were assigned a reliable redshift quality of 4. In order to improve the redshift reliability and uncertainties, and thus the group catalogue measurements, a fully automatic code was developed called AUTOZ.

Here we describe the AUTOZ algorithm, which uses a cross-correlation method that works equally well with absorption or emission line templates, and that is robust to additive/subtractive residuals and other uncertainties in the reduction pipeline that outputs the spectra. This has substantially improved the GAMA redshift reliability and velocity errors (Liske et al. in preparation). A description of the GAMA data is given in § 2. The method for finding the best redshift estimate is outlined in § 3, the quantitative assessment of the confidence is described in § 4, and the redshift uncertainty estimate is described in § 5. A summary is given in § 6.

2 DATA

The GAMA survey is based around a highly complete galaxy redshift survey and multi-wavelength database (Driver et al. 2011).

Since the initial spectroscopic target selection over 144 deg^2 described in Baldry et al. (2010), the survey has been expanded to 280 deg^2 with a main survey limit of $r < 19.8$ in all five regions: equatorial fields G09, G12 and G15 and Southern fields G02 and G23. The spectra were obtained from the Anglo-Australian Telescope with the Two-degree Field (2dF) robotic positioner fibre feed to the AAOmega spectrograph. In total, 286 705 spectra of 237 822 unique targets were taken over six years, in all weather conditions. The spectra were reduced using 2DFDR (Croom, Saunders, & Heald 2004). The GAMA setup and data processing details are described in Hopkins et al. (2013).

In order to obtain high completeness, both in targeting and redshift success, the same region of the sky was observed multiple times with different AAOmega configurations (Robotham et al. 2010). The spectra were reduced using 2DFDR and redshifts were measured using RUNZ typically within 24 hours of the observations. In between observing seasons, the spectra were usually re-reduced using the most recent update to the 2DFDR pipeline processing. In addition, a significant fraction of spectra were looked at by multiple users in order to quantify the reliability of the RUNZ redshift assignments (Liske et al. in preparation). The tiling catalogue was updated during an observing season, or in between observing seasons, using the latest assigned redshift qualities. If a target was not assigned a sufficient redshift quality and had not been observed twice by AAOmega, then it remained at high priority in the tiling catalogue. In most cases, a target received a higher-quality redshift on its second attempt.

Fig. 1 shows the distribution of fibre magnitudes of the GAMA targets that were observed by AAOmega (most targets with high quality redshifts from SDSS or 2dFGRS were not observed), and the mean number of AAOmega observations as a function of fibre magnitude. At bright fibre magnitudes, only a few per cent of targets were observed twice because they were first observed in poor conditions or for quality control purposes. At fainter fibre magnitudes, the number of targets observed more than once is higher because, even in average or good conditions, the RUNZ user was assigning a low quality redshift. Thus the strategy has worked, as expected, to obtain more observations for the fainter targets. As a result of the strategy, we have repeat observations of 40 319 targets. These repeats have been used to fine tune a new fully automatic redshift code called AUTOZ, and can be used for coadding to increase the spectral signal-to-noise ratio. This has significantly improved the redshift measurements with respect to the user assigned redshifts from RUNZ (Liske et al. in preparation).

3 REDSHIFT MEASUREMENTS

The code AUTOZ uses the cross-correlation method for obtaining redshifts for spectra with or without strong emission lines. It is described as a *fait accompli*, but there have been several iterations, each time checking to see if changes to the code resulted in an improvement. The tuning of parameters was optimised for performance with the AAOmega spectra. After each iteration, for example, redshift confidence estimates were calibrated from the repeat observations, the total number of high confidence redshifts was determined, and selected spectra and cross-correlation functions were inspected.

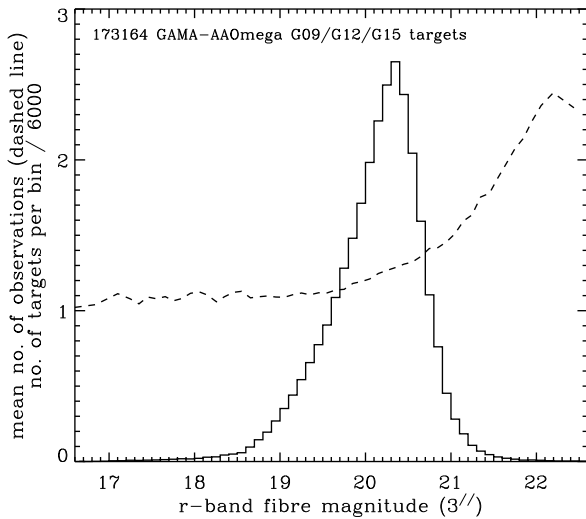


Figure 1. The distribution in the fibre magnitude of targets observed as part of the GAMA-AAOmega campaign (solid line), and the mean number of observations as a function of fibre magnitude (dashed line), for the equatorial fields. The fibre magnitudes were obtained from the SDSS catalogue.

3.1 Spectral templates

The SDSS has set a high standard for automatic redshift determination. For AUTOZ, we used their templates for spectral cross-correlation. These are a high S/N set of coadded spectra given in a similar format to the SDSS spectra for scientific targets. Table 1 lists the templates used for this paper. Twenty stellar spectra were used. Early versions of AUTOZ used the six SDSS DR2 galaxy templates (SubbaRao et al. 2002), while later versions used eight galaxy templates that were created from the SDSS-BOSS galaxy eigenspectra (Bolton et al. 2012). Six of these templates were chosen to closely match the DR2 templates where there was common wavelength coverage, with an additional two selected to represent a post-starburst spectrum (Wild et al. 2007) and a typical SDSS-BOSS spectrum.

The spectra were available rebinned onto a vacuum wavelength scale separated by 0.0001 in $\log_{10} \lambda$. This corresponds to a pixel size of 0.92 \AA at 4000 \AA and 1.84 \AA at 8000 \AA .

The spectral templates were high-pass filtered using a two step robust procedure:

(i) A 4th-order polynomial was fitted to the spectrum iteratively, with a maximum of 15 iterations. After each iteration, points more than 3.5σ away from the best-fit curve were rejected. The final 4th-order polynomial was then subtracted from the spectrum.

(ii) A median kernel filter of width 51 was applied to the result of the 1st step. On each end, the 25 edge points were given a median value of those points. This median filtered spectrum was smoothed using a trapezium filter, by applying two boxcar smooths of width 121 and 21. This low-pass spectrum was then subtracted from the result of the 1st step to obtain the high-pass filtered (HPF) spectrum.

The aim of the first step was to remove the large-scale modes from the spectrum so that the second step involving median filtering was not compromised by a steeply rising spectrum, for example. The HPF spectra also had their edge points set smoothly to zero using a cosine bell taper (apodization, Kurtz & Mink 1998). The chosen or maximum wavelength coverage of each template is given in Ta-

ble 1. A demonstration of the method is shown in Fig. 2 for the old-stellar galaxy template number 23.

The final HPF spectra for the templates were clipped to lie between -30 and $+30$ times the mean absolute deviation, determined iteratively until convergence within a small tolerance. An example of this is shown in Fig. 3. Here five emission lines are clipped. This is to avoid giving too much weight to a single strong line, which could give rise to cross-correlation spikes in bad data. In effect, a cross-correlation of this template with data gives a high peak when two or more lines line up with matched wavelength spacing. In other words, the correct wavelength spacing gives rise to higher confidence in the redshift with less weight given to the relative strengths of any lines.

We note that in SDSS DR8 onwards, the method for determining redshifts used χ^2 fitting with combinations of four eigenspectra for galaxies (Bolton et al. 2012). While we cannot follow their method for fitting because of the less reliable spectrophotometry of the AAOmega spectra, combinations of these eigenspectra were used to extend the wavelength range of the galaxy templates down to shorter wavelengths. These are templates 40–47 in the AUTOZ code, in order of increasing strength of emission lines.¹

3.2 AAOmega spectra

The AAOmega pipeline produces a spectrum and error spectrum for each target, with the red and blue beams combined to a single linear scale with a pixel width of 1.036 \AA . These were then approximately flux calibrated to relative f_λ units using an average flux correction determined for the survey. The reason for doing this is that the SDSS spectral templates are calibrated in f_λ units; and even though the spectra are high-pass filtered, the weighting is affected by the calibration.²

The AAOmega spectra for the GAMA survey were high-pass filtered in the same way as the spectral templates. The cosine bell taper was set between 3786 and 3736 \AA at the low-wavelength end and between 8790 and 8840 \AA at the high-wavelength end. Each error spectrum was broadened using a maximum filter kernel of width 3. This broadening allows for the uncertainty in the alignment of sky subtraction. In other words, this is to account for underestimation by $2DFDR$ of the error spectrum near sky lines. The HPF spectrum was then divided by the square of the error spectrum. This weighting was justified by Saunders et al. (2004) as appropriate for effectively minimising χ^2 when finding the peak. Fig. 4 shows the filtering procedure applied to an AAOmega spectrum.

The high-pass filtering is aggressive for both the templates and AAOmega spectra. This is to mitigate against artefacts on the scale

¹ We have chosen not to use quasar templates at this stage because of the significantly different scale and frequency of the features; they probably account for less than one per cent of the GAMA main sample. The confidence estimate for quasar redshifts is more difficult to make automatically when there is only one or two broad emission lines across the observed wavelength range. In addition, AAOmega spectra sometimes show an unfortunate broad artefact at the join between the red and blue arms, which may be confused with a broad line.

² We do not use the flux calibration applied to each AAOmega configuration separately (Hopkins et al. 2013). This fails in a few per cent of cases and may introduce incorrect flux variations across the spectra in other cases. Instead a robust, quadratic function, average flux calibration was determined and applied to all the unflux-calibrated spectra. In any case, flux calibration is not critical for cross-correlation and only affects the relative weighting between different parts of a spectrum.

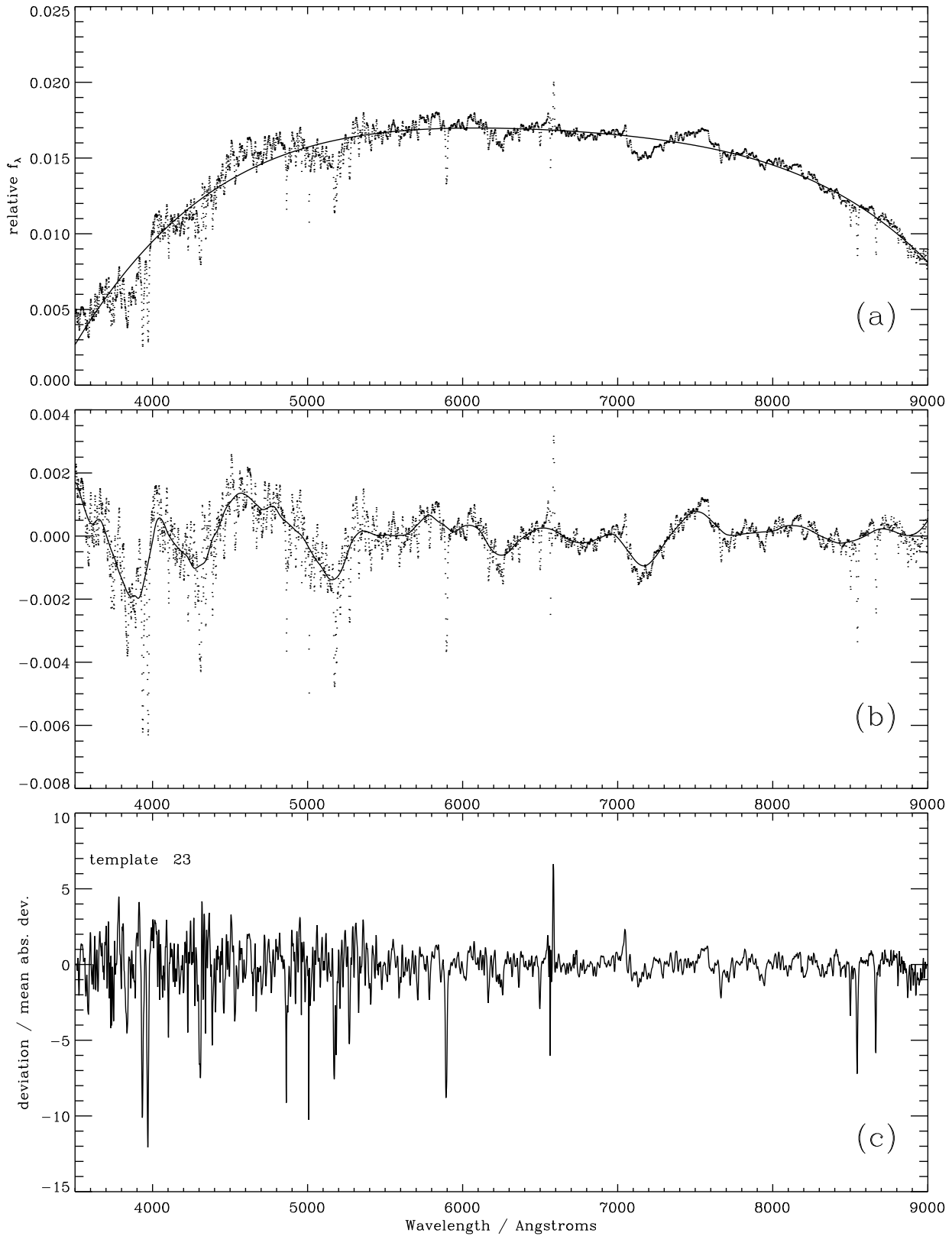


Figure 2. The high-pass filtering procedure for template 23. (a) The template spectrum is shown by the points, and the initial polynomial fit by the line. (b) The spectrum subtracted by the polynomial is shown with points, and the median filtered and smoothed version is shown by the line. (c) The final HPF template spectrum.

Table 1. Spectral templates used for cross correlation. The O-star and L1-star stellar templates were not included because they have negligible chance of genuine matches with our GAMA sample. For the AUTOZ redshifts used by the GAMA team, the initial database versions (SpecCat v20, v21) used 20 stellar and 6 galaxy templates (23–28), while later versions used 20 stellar and 8 galaxy templates (40–47). In either case, the galaxy templates cover a range of emission-line strengths relative to the absorption lines.

template numbers	file	spectral types	rest-frame $\lambda/\text{\AA}$	search z range	noise-estimate z range
02–10	spDR2-...	B to K stars	3800–9150	–0.002 to 0.002	–0.1 to 0.5
11–14, 17, 19, 22	spDR2-...	late-type stars	3800–9150	–0.002 to 0.002	–0.2 to 0.4
16, 18, 20, 21	spDR2-...	other stars	3800–9150	–0.002 to 0.002	–0.1 to 0.5
23–27	spDR2-...	galaxies	3500–9000	–0.005 to 0.8	–0.1 to 0.8
28	spDR2-028	luminous red galaxy	3000–6800	–0.005 to 0.8	–0.1 to 0.8
40–47	spEigenGal-55740	galaxies	2500–9000	–0.005 to 0.9	–0.1 to 0.9

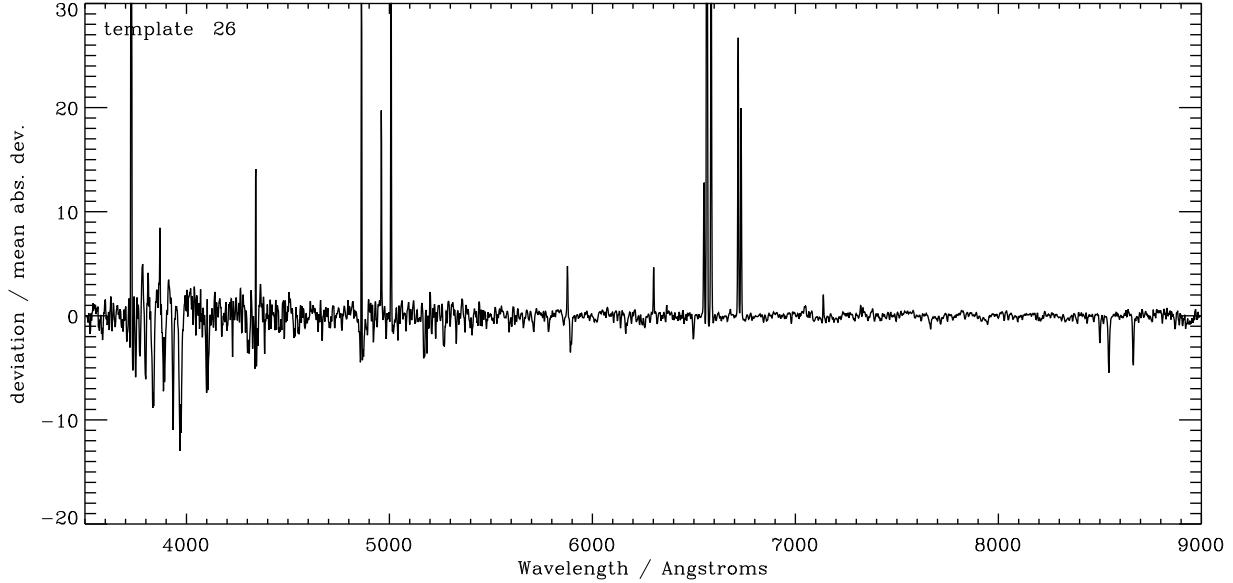


Figure 3. The high-pass filtered spectrum for template 26. The emission lines are clipped to 30 times the mean absolute deviation.

of around 200 \AA and longer, for example, ‘fringing’ caused by a separation between the prism and optical fibre at the 2dF plate, and an imperfect join between the spectra from the red and blue arms of the spectrograph (see Hopkins et al. 2013 for details). It is more straightforward to define a reliable automatic confidence estimate using HPF spectra where these scales have been removed.

The HPF spectra were then clipped to lie between -25 and 25 times the mean absolute deviation.³ This was chosen so that, in general, only high S/N spectra had genuine lines clipped. In these cases, the clipping does not compromise the cross-correlation peak position significantly because there is more than sufficient signal in less extreme deviations in any case. The clipping of the templates and AAOmega HPF spectra means that no single emission line, or apparent emission line, can result in a high confidence redshift. This approach is therefore more robust to bad data: uncorrected hot pixels, cosmic rays, or misaligned sky subtraction. Bad pixels that had been accounted for were set to zero in the HPF spectra.

³ The clipping limits were initially ± 30 , which were the same as those used for the templates. They were changed to ± 25 to alleviate some redshift disagreements between matched spectra at high figure-of-merit values (§ 4).

3.3 Cross-correlation functions

The template and target HPF spectra were linearly rebinned onto a logarithmic vacuum wavelength⁴ scale from 3.3 to 4.0 (with zero padding, Kurtz & Mink 1998) with a pixel width of 2×10^{-5} , which corresponds to 13.8 km/s . For each target HPF spectrum, the cross-correlation function was determined for all the templates using the usual procedure involving fast Fourier transforms (Simkin 1974). The cross-correlation values were associated with heliocentric redshifts given by

$$z_{\text{ccf},i} = 10^{(2 \times 10^{-5} \delta_{\text{pix},i})} (1 + z_t) \left(1 + \frac{v_{\text{sun},c}}{c} \right) - 1 \quad (1)$$

where $\delta_{\text{pix},i}$ is the shift in pixels corresponding to position i ; z_t is the redshift of the template spectrum, usually zero; and $v_{\text{sun},c}$ is component of the velocity of the Earth in the heliocentric frame to-

⁴ When converting the AAOmega spectra to a vacuum wavelength scale, the formula on the SDSS web pages was used: $\lambda_{\text{air}} = \lambda_v / (1.0 + 2.735182 \times 10^{-4} + 131.4182 / \lambda_v^2 + 2.76249 \times 10^8 / \lambda_v^4)$. A lookup table was created for the conversion factor as a function of λ_{air} , and the values determined for the AAOmega wavelengths by interpolation. The conversion factor varies between 1.000275 and 1.000285.

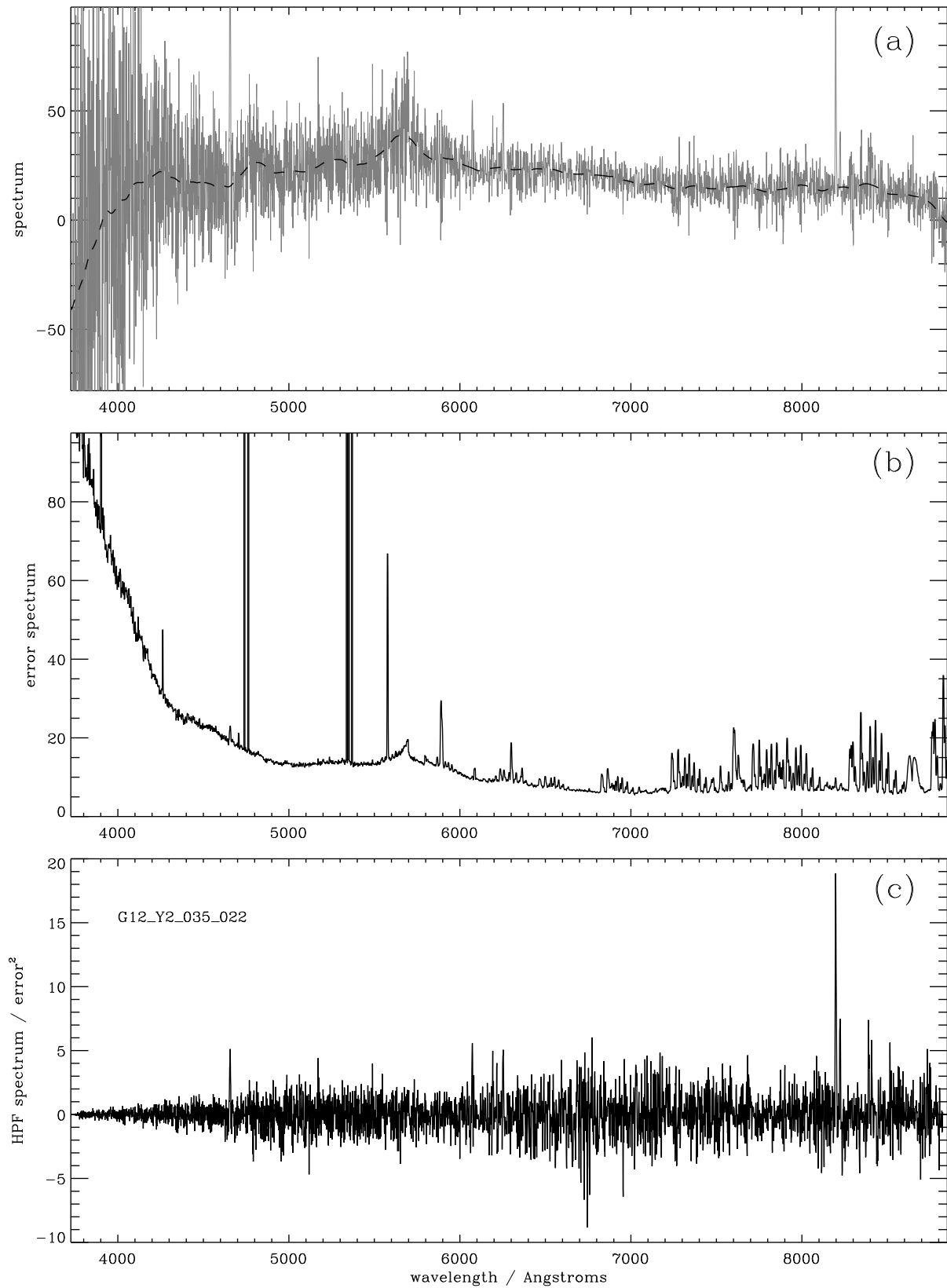


Figure 4. The high-pass filtering procedure for the AAOmega spectra. (a) The spectrum is shown in grey with the low-pass spectrum, to be subtracted from the spectrum, shown by the dashed line. (b) The uncertainty in the spectrum. Known bad pixels are represented by off-the-scale values giving rise to the spikes. (c) The final HPF spectrum to be used to produce cross-correlation functions.

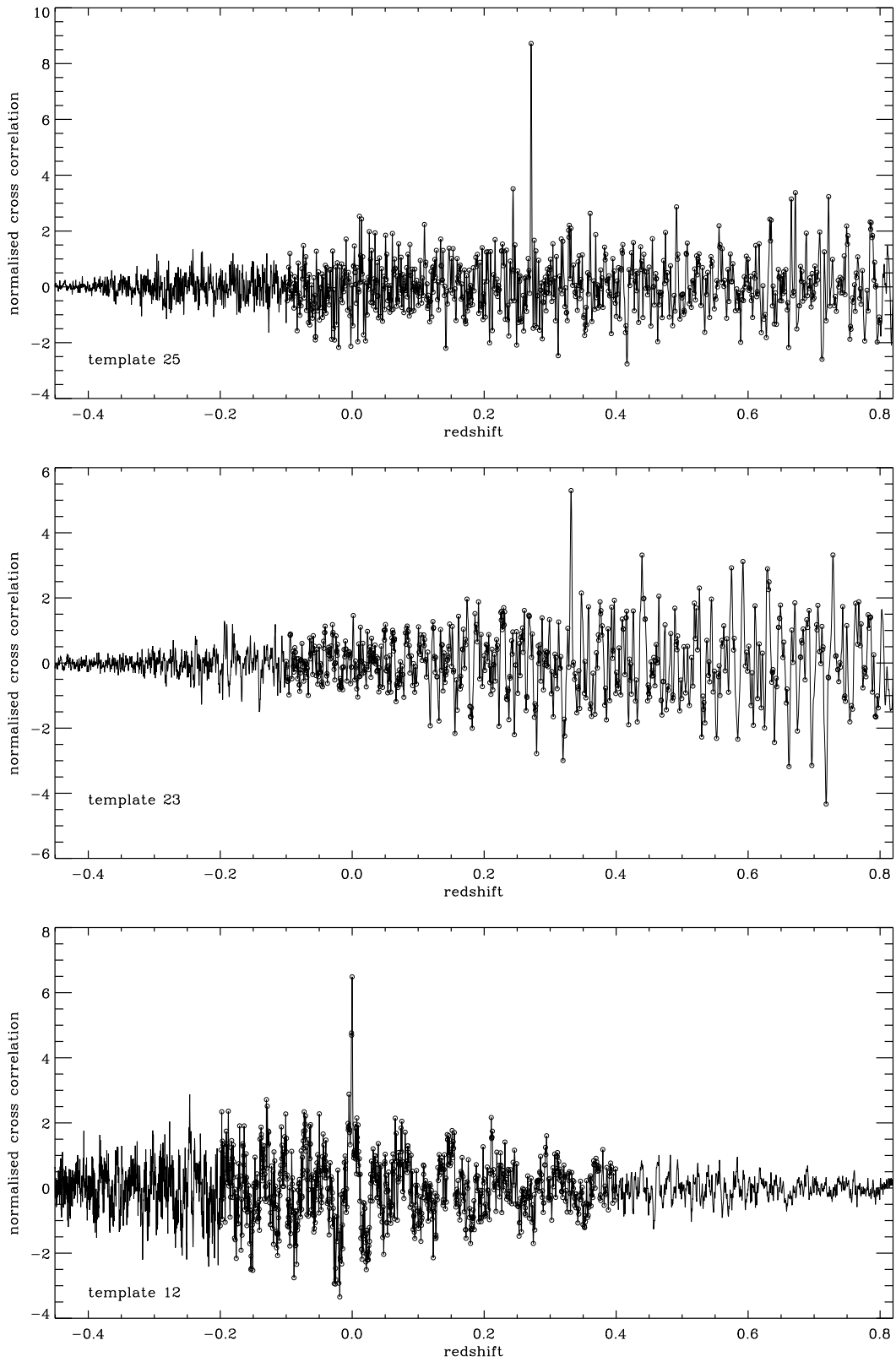


Figure 5. Examples of cross-correlation functions. The circles show the turning points and range used for the normalisation.

ward the target (if the target spectrum was not put on a heliocentric wavelength scale).

For each template, a search range for finding redshifts and a noise-estimate redshift range for the normalisation procedure were defined. The ranges for each template are given in Table 1. The cross-correlation functions were normalised by subtracting a truncated mean computed over the noise-estimate range, which results in a small adjustment, and dividing by the root mean square (RMS) of the turning points computed over the same range. Typically the cross-correlation functions had between 350 and 850 turning points over the noise-estimate range. Fig. 5 shows three examples of normalised cross-correlation functions.

For each target spectrum, all the normalised cross-correlation functions were determined corresponding to each template being used (26 or 28 templates; see Table 1). First, the highest cross-correlation peak, within the search ranges, was taken to be the best estimate of the redshift. The next three best redshifts were determined after excluding peaks within 600 km/s of the better redshift estimates, considering all templates, at each stage. The values of the peaks are called r_x (following the nomenclature of Cannon et al. 2006), $r_{x,2}$, $r_{x,3}$ and $r_{x,4}$ each with a corresponding redshift and template number. In order to avoid discretisation at the rebinned resolution, the redshifts were fine tuned by fitting a quadratic to seven points centred on each peak. Note that the highest redshift allowed was set at 0.9, which is appropriate for the GAMA magnitude limit and the fact that the AUTOZ code has not been adapted to search for quasar redshifts.

3.3.1 Note on the redshift range used for the normalisation

In order that the normalised cross-correlation functions, r_x values, can be compared between different templates, it is important that the noise-estimate ranges are set appropriately. The cross-correlation function computed using fast Fourier transforms gives values for $z_{ccf,i}$ from $10^{-0.35} - 1$ to $10^{0.35} - 1$ (about -0.55 to 1.24) because of the rebinned logarithmic scale from 3.3 to 4.0. Zero padding is necessary because of the wrap-around assumption of this cross-correlation method. As a result, the amplitude of a cross-correlation function can drop significantly when the overlap between the rest-frame wavelength range of the template (Table 1) and the observed wavelength range of the target decreases. Thus a more useful estimate of the noise is obtained by computing the RMS over a reduced redshift range, here called the noise-estimate range. The noise-estimate range for the galaxy templates is chosen to encompass the search redshift range with additional negative redshifts. The noise-estimate range for the stellar templates covers a shorter range because of the reduced rest-frame wavelength coverage. For late-type stars, the noise estimate uses more negative redshifts because there are larger deviations at the red-end of the template spectra. As a final test of the normalisation procedure, using repeated observations or otherwise, it can be apparent if certain templates give rise to numerous false redshift peaks (§ 4).

4 REDSHIFT CONFIDENCE ESTIMATION

In this section, we discuss the process for estimating the likelihood that the highest normalised cross-correlation peak corresponds to the correct redshift. In cases where the distribution of the cross-correlation function values of the turning points is close enough to Gaussian, then the value of r_x can be used to give an estimate of the redshift confidence (e.g. Cannon et al. 2006; see Heavens 1993

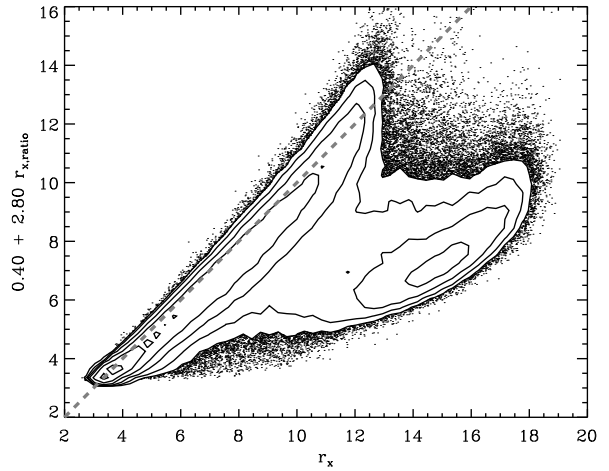


Figure 6. Bivariate distribution of $a_0 + a_1 r_{x,\text{ratio}}$ versus r_x . The solid lines represent logarithmically spaced density contours with a factor of two between each level. The dashed line shows where the two values are equal.

for a theoretical estimate). However, in most cases, there are a few high values of the cross-correlation functions because of aliasing between emission lines, for example. To test the reliability of the best redshift estimate, we also consider the ratio between the highest peak and the subsequent peaks, here, given by

$$r_{x,\text{ratio}} = \frac{r_x}{\sqrt{(r_{x,2})^2 + (r_{x,3})^2 + (r_{x,4})^2}}. \quad (2)$$

Fig. 6 shows the distribution of an adjusted $r_{x,\text{ratio}}$ versus r_x for 286 705 AAOmega spectra. Cross-correlations with the templates that have weak or no emission lines tend to follow the diagonal ridge line while spectra that have higher peaks using the emission lines dominate the hill to the right. Cross-correlations with noise populate the bottom left corner. Of the two variables, $r_{x,\text{ratio}}$ gives a better figure of merit (FOM) for relating to redshift confidence. A slight improvement can be made by defining the following:

$$cc_{\text{fom,prelim}} = \min(r_x, a_0 + a_1 r_{x,\text{ratio}}). \quad (3)$$

with $a_0 = 0.4$ and $a_1 = 2.8$, and where the $\min()$ function returns the lower of the two variables.⁵ The line where these variables are the same is shown in Fig. 6.

Three further adjustments, penalty functions, to the FOM were made. The first is because in cases of poor sky subtraction or other reduction problems, $cc_{\text{fom,prelim}}$ can still be above 5 even when there is no signal from the target source. For each HPF spectrum, the ratio of the RMS to mean absolute deviation (MAD) was determined. This value (rms/mad) is high when there is good signal from the target or when there is non-Poisson noise, i.e., reduction problems. Thus, the FOM can be reduced when $\text{rms}/\text{mad} > 1.8$ (the median value is 1.44) without losing genuine redshifts. The adjustment is given by

$$\text{adjust}_1 = \begin{cases} -2.1 & \frac{\text{rms}}{\text{mad}} > 3.2 \\ -1.5\left(\frac{\text{rms}}{\text{mad}} - 1.8\right) & 1.8 < \frac{\text{rms}}{\text{mad}} < 3.2 \\ 0 & \frac{\text{rms}}{\text{mad}} < 1.8 \end{cases}. \quad (4)$$

⁵ The slope of the line a_1 was determined by fitting to the ridge line. The value of a_0 was adjusted by trial and error to give the largest number of high confidence redshifts from the AAOmega spectra, after calibrating the confidence each time. In the absence of sufficient repeat spectra, fitting to the ridge line would provide an adequate estimate for an improved FOM.

The second adjustment is particular to the sample targeted. So far only a flat prior has been set for the allowed redshifts; this is given by the search ranges. However, there are far fewer galaxies at $z > 0.5$ than at lower redshifts in the GAMA survey. This adjustment is given by

$$\text{adjust}_2 = \begin{cases} -0.8 & z > 0.65 \\ -4.0(z - 0.45) & \text{for } 0.45 < z < 0.65 \\ 0 & z < 0.45 \end{cases}, \quad (5)$$

and thus

$$cc_{\text{fom}} = cc_{\text{fom,prelim}} + \text{adjust}_1 + \text{adjust}_2. \quad (6)$$

Finally, contamination by solar-system light was checked on a tile by tile basis,⁶ by looking for an excessive number of G-star template matches. The number of stars observed as part of our main survey is about two per cent (Baldry et al. 2010). When there was a clustering of ten or more matches to templates 7–10 (best or second-best redshift estimate), the tile was checked for solar-system contamination. This was caused by moonlight, under conditions where scattering had significant structure on the sub-tile scale, with one notable exception. A cluster of about twenty matches was found to be centred on the location of Saturn at the time of the observation. The spectrum of Saturn can be seen clearly in a few fibres; AUTOZ does not have this template but picks up the reflected solar absorption lines. In total, 20 tiles were flagged as having possible solar contamination, and any best redshift match to templates 7–10 was given a cc_{fom} value of 2.5. This was applied to about 300 spectra and these were not included in the redshift confidence estimation. In most cases, the targets were re-observed.

The calibration of cc_{fom} to a redshift confidence was made by comparing AUTOZ redshifts between different spectra of the same target position (matched spectra).⁷ Redshift measurements were considered to be in agreement if they were within 450 km/s [$\Delta \ln(1+z) < 0.0015$] and in disagreement otherwise. The probability of agreement is taken to be

$$p_{\text{agree}} = p(cc_{\text{fom},i})p(cc_{\text{fom},j}) \quad (7)$$

where the function $p()$ gives the probability each spectrum is correct as function of the FOM. This ignores the small chance that both redshifts are incorrect but in agreement with each other or that both redshifts are correct but are of different superimposed sources. The second effect was noticeable prior to suppression of the solar-system contamination.

In order to estimate $p(cc_{\text{fom}})$, two binned samples were considered. The first sample uses the matched spectra where one of the FOM values is higher by more than 1.0, and the sample is binned by the lower FOM value. In each bin the estimate of $p(cc_{\text{fom}})$ is then N_{agree}/N , which assumes the redshift is correct for the spectrum with the higher FOM value. The second sample uses the matched spectra where the FOM values are within 0.5 of each other, and the sample is binned by the mean value. In each bin the estimate of $p(cc_{\text{fom}})$ is then $\sqrt{N_{\text{agree}}/N}$, which assumes $p(cc_{\text{fom}})$ is the same for both spectra in a matched pair. Fig. 7 shows these binned estimates for the function.

The data were also fitted using a tanh function

⁶ A tile refers to the set of spectra from a single AAOmega configuration.

⁷ Observations of the same target taken with different 2dF configurations are of the same position on the sky within the accuracy of the fibre placement, which is $0.3''$. This is significantly less than the fibre diameter, which subtends $2''$ on the sky.

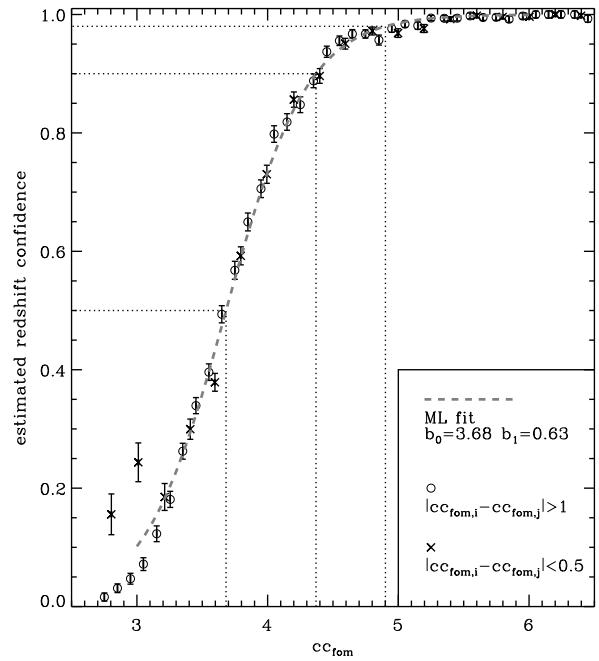


Figure 7. Estimate of the redshift confidence as a function of cc_{fom} . The circles represent the first binned sample where the FOM values between the matched spectra differ by more than 1.0, while the crosses represent the second binned sample where the FOM values are similar. The dashed line shows the parametric fit using a maximum likelihood method on the unbinned data. The dotted lines show the FOM values corresponding to redshift confidence of 0.5, 0.9 and 0.98.

$$p(x) = 0.5 \tanh\left(\frac{x - b_0}{b_1}\right) + 0.5. \quad (8)$$

The best fit parameters were determined by maximising the likelihood:

$$\ln P = \sum_{i,j,\text{agree}} \ln[p(cc_{\text{fom},i})p(cc_{\text{fom},j})] + \sum_{i,j,\text{disagree}} \ln[1 - p(cc_{\text{fom},i})p(cc_{\text{fom},j})] \quad (9)$$

where the summations are over matched spectra with redshift agreement and disagreement. The best fit was found using only the matched spectra where the lower FOM value within each pair was between 3.0 and 6.0. This is shown by the dashed line in Fig. 7.

Various subsamples of the matched spectra were also considered including a randomly selected repeat sample (these were targets that were chosen for reobservation regardless of their assigned redshift quality), and subsamples where one of the spectra had a particular best-match template. The calibration points for the subsamples, at which the redshift confidence was 0.9, varied from $cc_{\text{fom}} \simeq 4.2$ to 4.6. The notable exception was where one of the matched spectra had a stellar template match. Here there were a higher fraction of disagreements at $cc_{\text{fom}} > 5$ than in other subsamples (0.9 confidence at 5.2). This is a result of star-galaxy blends and is not of concern for the AUTOZ method. The GAMA target selection is for extended sources, and thus it is not surprising that a higher fraction of targets with stellar redshifts are part of a star-galaxy blend compared to random selection; in addition spectra of star-galaxy blends are more likely to have been reobserved given the increased difficulty of assigning redshifts using RUNZ. Overall, we use $b_0 = 3.7$ and $b_1 = 0.7$ to assign redshift confidence, which is slightly more conservative than the best fit to all the matched spectra (Fig. 7).

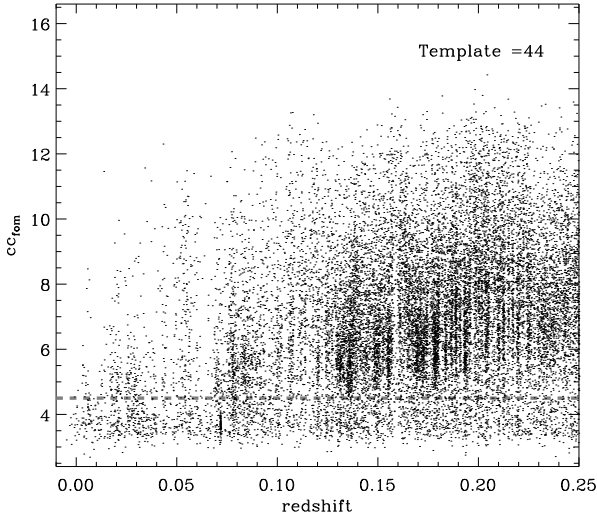


Figure 8. Example diagnostic plot of cc_{fom} versus redshift. The dashed line shows the standard cut to select sufficient quality redshifts.

After the redshift confidence calibration, 248 145 spectra were assigned a probability $p(cc_{fom}) > 0.9$ (AATSpecAutozAllv22, which uses the galaxy templates 40–47). The mean calibrated confidence using this quality selection is 0.996 implying that less than 1% would be assigned an incorrect redshift. For this and earlier versions, additional diagnostics were run to check for anomalies including: checks for solar-system contamination (described earlier), plots of spec- z versus photo- z for every tile, plots of matched spectra where there was redshift disagreement with $cc_{fom} > 5$ for both, and plots of cc_{fom} versus z for each template. An example of the latter is shown in Fig. 8. The cut at $cc_{fom} = 4.5$ corresponds approximately to our standard quality cut ($p > 0.9$). One can see the redshift spikes corresponding to large-scale structure above the line, with more scatter below the line. There is a narrow artefact below the line at $z \simeq 0.0715$. In previous iterations of the AUTOZ code, poor sky subtraction, for example, was evident with signatures of serious artefacts extending from below to above the quality cut. These artefacts were eliminated by changes to the code (e.g., broadening of the error spectrum), and by improved reduction of several tiles.

4.1 Redshift completeness of the GAMA equatorial fields

The large number of targets with two or more spectra taken has allowed the AUTOZ code to be accurately calibrated. However, the main aim of the repeated observations was simply to obtain high redshift completeness. If a target was first observed in poor conditions or using a fibre with lower than average transmission efficiency, then the second observation was often successful in obtaining a redshift.

To demonstrate the effect of the strategy on the redshift completeness, we select the sample of main sample targets in the G09, G12 and G15 that have been observed at least once with AAOmega (as per Fig. 1).⁸ Fig. 9 shows the redshift completeness as a function of fibre magnitude. The dotted line shows the completeness

⁸ The main sample targets are predominantly $r_{petro} < 19.8$ with good visual classification. The sample has been cleaned of SDSS database objects where the photometry looks to be significantly in error. The number of main

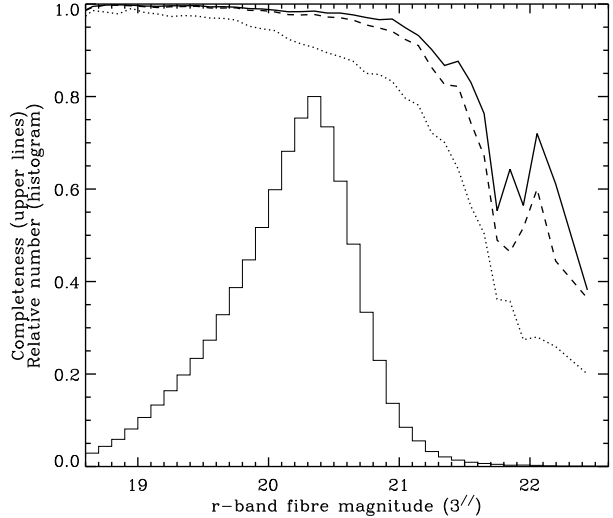


Figure 9. Redshift completeness as a function of fibre magnitude for main survey targets (top three lines) using: the first observation of any target (dotted line), the best observation (dashed line), and incorporating coadded observations (solid line). The histogram of fibre magnitudes is also shown (lower solid line).

($p > 0.9$) if only the first observation is used for each target (or a pre-existing good redshift), while the dashed line shows the completeness using the best observation. Note the significant improvement when poor quality observations are replaced.

For some targets that are intrinsically faint, a further improvement can be made by coadding any repeated observations. In principle, spectra should be coadded in proportion to their signal divided by their noise squared. In reality, it is hard to estimate the signal because of the faintness and sometimes poor sky subtraction. Since we will only obtain a significant improvement in the FOM if the signal-to-noise ratio is similar for two spectra that are summed together, we assume that this is the case. The spectra to be summed were high-pass filtered and normalised, as per Fig. 4 and § 3.2, separately. The HPF spectra were then rebinned onto a heliocentric vacuum wavelength scale before summing. The AUTOZ cross-correlation and redshift confidence estimation was then run on the summed HPF spectra. The solid line in Fig. 9 shows the resulting increase in completeness when low confidence single-spectrum redshifts are replaced by coadded-spectrum redshifts where there is an improvement in the FOM. Overall, the fraction of the GAMA main sample with $p > 0.9$ AUTOZ redshifts is 98.3%. The mean p -value after selecting on this redshift quality cut is 0.992.

5 REDSHIFT UNCERTAINTIES

In this section, we discuss the measurement uncertainty assuming that the correct redshift peak has been assigned. This uncertainty comes from errors in wavelength calibration, noise affecting the centroid of the peak and mismatch between the template and observed spectra. To test this we take the sample of matched spectra where the redshifts are in agreement (within 450 km/s) and both

sample targets is 191 051 in the equatorial fields, of which, 173 164 have AAOmega observations (TilingCatv42).

have $cc_{\text{fom}} > 3.5$ but with the redshift peaks coming from *different* galaxy templates. This gives a sample of 12 323 matched spectra.

Following Tonry & Davis (1979) and from trial and error, a reasonable predictor of the ability to centroid is given by

$$\mathcal{V} = \frac{v_{\text{fwhm}}}{1 + r_x} \quad (10)$$

where v_{fwhm} is the velocity full-width half maximum of the peak. The latter is determined from the number of rebinned pixels (13.8 km/s) within 600 km/s of the peak above the half maximum of the cross-correlation function. This is more robust and less time consuming than fitting a Gaussian or other function to the peak. Overall, we model the variance in the velocity (redshift) uncertainty as:

$$\sigma_v^2 = \left(c \frac{\sigma_z}{1+z} \right)^2 = c_0^2 + c_1^2 \mathcal{V}^2 \quad (11)$$

Thus the expected mean square of the velocity difference between matched spectra i and j is given by

$$\langle \Delta v_{i,j}^2 \rangle = 2c_0^2 + c_1^2 (\mathcal{V}_i^2 + \mathcal{V}_j^2) \quad (12)$$

Fig. 10 shows the velocity difference ($|\Delta v_{i,j}|$) versus the predictor value $\sqrt{\mathcal{V}_i^2 + \mathcal{V}_j^2}$. This shows that the mean velocity difference increases with average \mathcal{V} as expected. The mean square values of the velocity differences were determined in bins of the predictor value. These binned values are shown in the figure (plotted as three times the RMS value) and were used to determine c_0 and c_1 using a fit between 45 and 260. Over this range, the fit is good and thus is expected to give a reasonable estimate of σ_v . The fit overpredicts the velocity difference at predictor values less than 45. These correspond to spectra with strong emission lines. For the purposes of group dynamical measurements, it is more important to have an accurate measure of the velocity uncertainty when this uncertainty is larger and thus we apply the fit to all the GAMA-AAOmega spectra. For the high quality redshift sample ($p > 0.9$), the median σ_v is 33 km/s, with 85 per cent of redshifts having an uncertainty less than 50 km/s using this calibration. Fig. 11 shows the distribution of velocity uncertainty as a function of the fibre magnitude.

5.1 Comparison with SDSS DR10

At the start of the GAMA spectroscopic campaign, SDSS DR7 and other pre-existing redshifts were matched to the input catalogue (Baldry et al. 2010). Since then SDSS has had three more data releases, including spectra from the BOSS survey (Dawson et al. 2013). In addition, the primary method of determining redshifts was updated to χ^2 fitting using eigenspectra (Bolton et al. 2012). This was applied retrospectively to all plates observed for the SDSS surveys.

In order to compare GAMA AUTOZ redshifts with SDSS, we selected all SDSS DR10 redshifts in the GAMA fields with ZWARNING=0 (primarily a reduced χ^2 difference of more than 0.010 between the 1st and 2nd redshift peaks). This corresponds approximately to $p > 0.9$ from our tests, and as implied by Bolton et al. (2012)'s test, which showed that as the χ^2 difference threshold was lowered to 0.008, 8% of the additional redshifts were estimated to be incorrect. Matching the SDSS ZWARNING=0 spectra from DR10 to the GAMA AAOmega spectra ($p > 0.9$, excluding spectroscopic standards) within 1 arcsec results in 9426 cross matches. From these, 99.1% have redshifts in agreement between GAMA and SDSS, which is as expected for a mean confidence of 99.5% for the GAMA sample and a similar value for the SDSS sample.

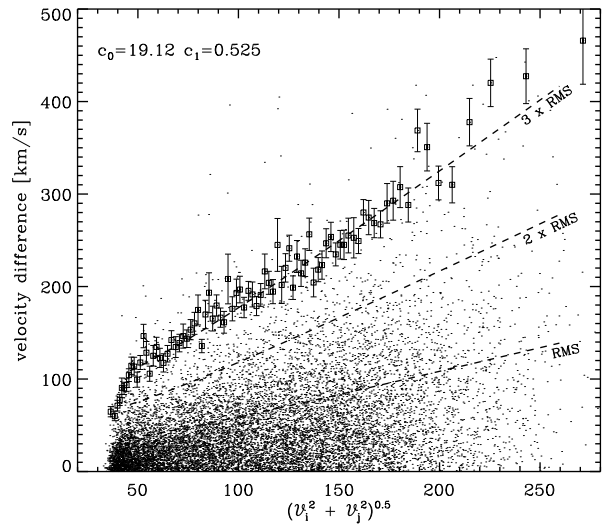


Figure 10. Velocity difference versus $\sqrt{\mathcal{V}_i^2 + \mathcal{V}_j^2}$. The points represent the $|\Delta v_{i,j}|$ values for the matched spectra. The squares, with error bars, show *three times* the RMS velocity differences in bins. The dashed lines show one, two and three times the RMS values using a fit for c_0 and c_1 (Eq. 12) between 45 and 260.

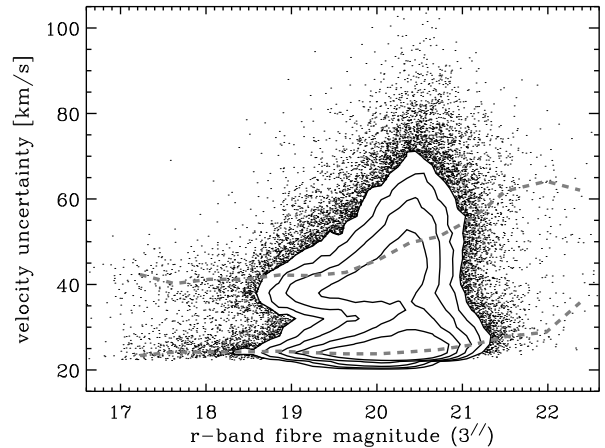


Figure 11. Calibrated velocity uncertainty as a function of the fibre magnitude. The GAMA-AAOmega sample distribution is shown by the points and solid-line contours, for the equatorial fields, while the 16th and 84th percentiles in bins of the fibre magnitude are shown by the dashed lines. The lower ridge corresponds primarily to spectra matched to templates with strong emission lines, while the ridge at about 40 km/s corresponds to spectra matched to templates with weak or no emission lines.

There are 1748 matches to spectra from the original SDSS spectrographs that were part of the legacy survey (main galaxy sample and luminous red galaxies). These matches were obtained for quality control purposes or because SDSS had reported a low redshift confidence in DR7. There are 7674 matches to spectra from the BOSS spectrographs and survey. The large number of matches is a result of GAMA and BOSS independently choosing these targets. Fig. 12 shows the velocity difference histogram for the two samples [$\Delta v_{i,j} = c \ln(1 + z_{\text{GAMA}}) - c \ln(1 + z_{\text{SDSS}})$]. For the legacy sample, the mean and standard deviation were 12 and 38 km/s, and for the BOSS sample, they were 5 and 53 km/s. The

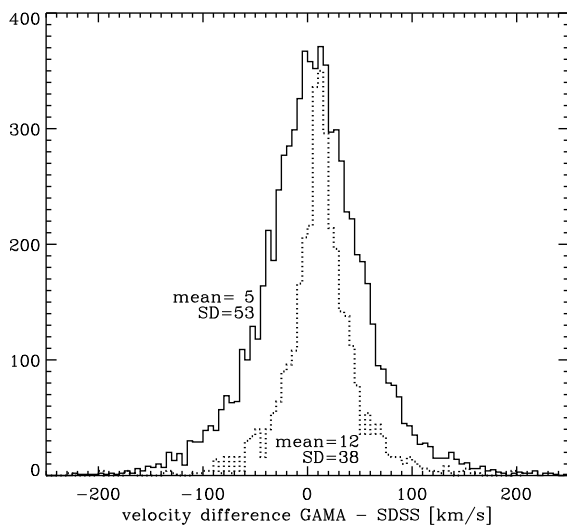


Figure 12. Velocity difference between GAMA and SDSS redshift measurements. The solid line shows the histogram for the SDSS-BOSS sample of galaxies, while the dotted line shows the histogram for the SDSS-legacy sample (histogram values scaled up by a factor of two).

standard deviations are as predicted from the velocity errors estimated above for GAMA, with a smaller contribution from SDSS as estimated by Bolton et al. (2012). The larger mean offset with respect to the legacy sample may be because of the different eigen-spectra used: spEigenGal-53724.fits as opposed to spEigenGal-55740.fits used by BOSS and GAMA AUTOZ. Other than this small anomaly, the comparison with SDSS supports the GAMA estimates of redshift confidence and velocity uncertainty described in this paper.

6 SUMMARY

We have developed a redshift measurement code called AUTOZ for use on the GAMA AAOmega spectra. The method uses the cross-correlation technique with robust high-pass filtering suitable for galaxy and stellar types applied to the templates (Fig. 2) and observed spectra (Fig. 4). The observed HPF spectra are inversely weighted by the variance estimated at each pixel, broadened slightly by a maximum kernel filter. To avoid giving too much weight to emission line matches, large deviations in the HPF spectra are partially clipped for both the observed spectra and templates (Fig. 3). Lowering the weight of large deviations reduces the impact of spurious peaks caused by uncorrected artefacts. Real cross-correlation peaks are rarely adversely affected by this because there is additional signal at the correct redshift peaks from other parts of the spectra.

For each observed spectrum, the cross-correlation functions are determined for every chosen template. Each function is normalized by dividing by the RMS of the turning points over a specified noise-estimate range (Table 1). These ranges were chosen so that the value of a peak represents a similar confidence level across all the templates. The best four redshift estimates are obtained from the cross-correlation function peaks (Fig. 5), not including peaks within 600 km/s of a better redshift estimate. A FOM for the redshift confidence is determined using the value of the highest peak (r_x), and the ratio of r_x to the RMS of the 2nd, 3rd and 4th peaks

(Eqs. 2–3, Fig. 6). Overall, the procedure can be adjusted and the FOM calibrated using repeat observations within a survey.

The GAMA AAOmega redshift survey has taken spectra of over 230 000 unique targets. As part of a strategy of obtaining high completeness and for quality control, about 40 000 targets have had two or more spectra taken. These repeats were used to calibrate the confidence level as a function of the FOM using a maximum likelihood method (Eqs. 8–9, Fig. 7). Overall, the AUTOZ code has significantly improved the redshift reliability within the GAMA main sample, with a high completeness for targets with 3''-aperture r -band magnitudes as faint as 21 mag (Fig. 9). The redshift uncertainties have also been calibrated using the repeat observations, with most having redshift errors less than 50 km/s (Fig. 11). AUTOZ measurements will be included in public data releases from GAMA DR3 onwards.

With some consideration to making adjustments — templates, high-pass filtering scale, clipping limits, noise-estimate ranges, FOM calculation and calibration — the fully automatic method outlined here could be used for other large galaxy redshift surveys. A key factor is using a sufficient number of repeats, both random and at the fainter end of the sample, to allow for an accurate empirical confidence calibration.

ACKNOWLEDGEMENTS

Thanks to the anonymous referee for helpful comments on the manuscript. The AUTOZ code makes use of routines from the IDL Astronomy User's Library. GAMA is a joint European-Australasian project based around a spectroscopic campaign using the Anglo-Australian Telescope. The GAMA input catalogue is based on data taken from the Sloan Digital Sky Survey and the UKIRT Infrared Deep Sky Survey. Complementary imaging of the GAMA regions is being obtained by a number of independent survey programs including GALEX MIS, VST KiDS, VISTA VIKING, WISE, Herschel-ATLAS, GMRT and ASKAP providing UV to radio coverage. GAMA is funded by the STFC (UK), the ARC (Australia), the AAO, and the participating institutions. The GAMA website is <http://www.gama-survey.org/>.

REFERENCES

- Aihara H., et al., 2011, *ApJS*, 193, 29
- Baldry I. K., et al., 2010, *MNRAS*, 404, 86
- Beers T. C., Flynn K., Gebhardt K., 1990, *AJ*, 100, 32
- Bolton A. S., et al., 2012, *AJ*, 144, 144
- Cannon R., et al., 2006, *MNRAS*, 372, 425
- Colless M., et al., 2001, *MNRAS*, 328, 1039
- Croom S., Saunders W., Heald R., 2004, *Anglo-Australian Observer Newsletter*, 106, 12
- Dahlen T. et al., 2013, *ApJ*, 775, 93
- Dawson K. S., et al., 2013, *AJ*, 145, 10
- Driver S. P., et al., 2009, *Astron. Geophys.*, 50, 5.12
- Driver S. P., et al., 2011, *MNRAS*, 413, 971
- Faber S. M. et al., 2003, *Proc. SPIE*, 4841, 1657
- Garilli B., Fumana M., Franzetti P., Paioro L., Scodreggio M., Le Fèvre O., Paltani S., Scaramella R., 2010, *PASP*, 122, 827
- Glazebrook K., Offer A. R., Deeley K., 1998, *ApJ*, 492, 98
- Heavens A. F., 1993, *MNRAS*, 263, 735
- Hopkins A. M. et al., 2013, *MNRAS*, 430, 2047
- Kaiser N., 1987, *MNRAS*, 227, 1

- Kurtz M. J., Mink D. J., 1998, *PASP*, 110, 934
- Kurtz M. J., Mink D. J., Wyatt W. F., Fabricant D. G., Torres G., Kriss G. A., Tonry J. L., 1992, in *Astron. Soc. Pacific Conf. Ser.*, Vol. 25, *Astronomical Data Analysis Software and Systems I*, Worrall D. M., Biemesderfer C., Barnes J., eds., p. 432
- Le Fèvre O. et al., 2003, *Proc. SPIE*, 4841, 1670
- Lewis I. J., et al., 2002, *MNRAS*, 333, 279
- Mink D. J., Wyatt W. F., 1995, in *Astron. Soc. Pacific Conf. Ser.*, Vol. 77, *Astronomical Data Analysis Software and Systems IV*, Shaw R. A., Payne H. E., Hayes J. J. E., eds., p. 496
- Newman J. A. et al., 2013, *ApJS*, 208, 5
- Robotham A., et al., 2010, *Publ. Astron. Soc. Australia*, 27, 76
- Robotham A. S. G. et al., 2011, *MNRAS*, 416, 2640
- Saunders W., Cannon R., Sutherland W., 2004, *Anglo-Australian Obser. Newsletter*, 106, 16
- Sharp R., et al., 2006, *Proc. SPIE*, 6269, 62690G
- Simkin S. M., 1974, *A&A*, 31, 129
- Smee S. A. et al., 2013, *AJ*, 146, 32
- Stoughton C., et al., 2002, *AJ*, 123, 485
- SubbaRao M., Frieman J., Bernardi M., Loveday J., Nichol B., Castander F., Meiksin A., 2002, *Proc. SPIE*, 4847, 452
- Tonry J., Davis M., 1979, *AJ*, 84, 1511
- Wild V., Kauffmann G., Heckman T., Charlot S., Lemson G., Brinchmann J., Reichard T., Pasquali A., 2007, *MNRAS*, 381, 543